Nonlinear Dyn (2011) 63: 19–33
DOI 10.1007/s11071-010-9782-7

ORIGINAL PAPER

Virtual orbits and two-parameter bifurcation analysis in a ZAD-controlled buck converter

Viktor Avrutin · Enric Fossas · Albert Granados · Michael Schanz

Received: 30 November 2009 / Accepted: 11 July 2010 / Published online: 8 August 2010

Abstract Based on a recently obtained Lemma about periodic orbits in linear systems with a piecewise-linear non-autonomous periodic control, we describe analytically the bifurcation structures in a ZAD-controlled buck converter. This analytical description shows that the period doubling bifurcation in this system may be both subcritical or supercritical. Considering virtual orbits we show how a saddle-node bifurcation becomes feasible and how it is destroyed at a new codimension-2 bifurcation point, where the subcritical period doubling bifurcation becomes supercritical. We also show that this phenomenon does not take place when the error surface in the ZAD conditions piecewise-linear defined.

Keywords Non-smooth systems · Bifurcations · Virtual orbits · Zero average dynamics · Control · Power electronics

This work was supported in part by the DAAD-La Caixa's Grant Program, the Ministerio de Ciencia y Tecnología, Spain, through Grant DPI2007-62582 and by the European Union (FEDER).

V. Avrutin · A. Granados (✉) · M. Schanz
IPVS, University of Stuttgart, Stuttgart, Germany
e-mail: albert.granados@ipvs.uni-stuttgart.de

E. Fossas
IOC-ESAII, Universitat Politècnica de Catalunya, Barcelona, Spain

1 Introduction

Nowadays, due to the increasing use of mobile electronic devices and to the avoiding fuel tendency, the use of batteries is being more and more extended. Energy saving demands not only enhanced efficiency in these power supply devices, but also a more accurate control of the conversion of the voltage obtained from the battery and the one requested by the electronic device. This conversion is achieved by a DC/DC power electronic converter applying two different circuits during specific times, and repeating this operation in a high frequency manner. The key aspect of the control of this device and therefore the quality of the desired voltage is the design of a *duty cycle* which determines these specific times and, in the most sophisticated cases, may vary with the system variables (usually a current and a voltage). The switching behavior of this converter leads to a model which is piecewise smooth on the right hand side (also called Filippov systems), and the repeating behavior makes the system non-autonomous but periodic. This property permits the use of averaging methods for the control design, such as working with the averaged system (see for instance [11]) or the use of the so-called ZAD strategy (zero average dynamics) extensively numerically, analytically and also experimentally studied in [2, 3, 5, 9].

In this work we consider a DC/DC buck converter controlled by a method based on the ZAD strategy, introduced by Biel and coworkers in [9], leading the control design the choice of a certain time constant. In the

two-dimensional parameter space defined by this time constant and the desired constant voltage not only phenomena typical for smooth systems as period doubling bifurcations but also corner collision bifurcations typical for non-smooth systems occur.

The interactions of smooth and non-smooth bifurcation phenomena has drawn the attention of many researchers and led them to investigate this kind of systems. Many authors investigating smooth and non-smooth bifurcation phenomena use the buck converter as paradigm (we refer to [8] for a comprehensive overview about the state of the art in this field). Recent studies [4, 10] performing a two-parameter bifurcation analysis of the ZAD-controlled buck converter show, that this parameter space has a rich and complex structure.

These studies focused on the use of two different control laws. The first one (*transcendental ZAD condition*) needs the duty cycle to be calculated through a transcendental equation which has to be solved at each step, but permits the use of theoretical results to perform an analytical study of the bifurcations [10]. The second one (*algebraic ZAD condition*) leads to an algebraic expression for the suitable duty cycle which permits an easier implementation in hardware and for simulations proposes, but the bifurcation phenomenon has to be investigated mainly numerically [4].

The period doubling and corner collision bifurcation curves reported in both works present qualitative differences. In [10] both curves cross at three codimension-2 bifurcation points leading them to change their relative position (as shown below in Fig. 3). By contrast, in [4] only two of these points exist so that the period doubling bifurcation curve remains on the right hand side of the corner collision bifurcation in the whole parameter space. Following [10], we present in this work analytical results showing that the period doubling bifurcation may be supercritical or subcritical leading the orbits emerging at this bifurcation to be stable or unstable, respectively, in different regions of the parameter space. By contrast to this, we show also that when using the algebraic ZAD condition, the period doubling bifurcation is supercritical for all parameter values. When dealing with the transcendental ZAD condition, we demonstrate that the transition from the supercritical to the subcritical period doubling bifurcation is associated with a saddle-node bifurcation. The saddle-node bifurcation curve originates from a point at the corner collision bifurcation curve and is destroyed where it collides with the period doubling curve. The characteristics of this bifurcation curve not only permits us to detect a new codimension-2 bifurcation point but also to explain the behavior of 2-periodic orbits near the other points of this type.

The saddle-node bifurcation leads us to distinguish between *feasible* and *virtual* orbits. Moreover, stable virtual 2-periodic solutions permit us to justify the existence of saturated 2-periodic orbits after the corner collision bifurcation, that is, 2-periodic orbits without switching behavior in one sampling period.

This paper is organized as follows. In Sect. 2 an introduction to the system and the ZAD condition is given. In Sect. 3 we present a brief review of the previous results, introduce the concept of virtual and feasible orbits and state our main results. In Sect. 4 we discuss numerical simulations in order to confirm the analytical results, and compare them additionally with the ones obtained when using the algebraic ZAD condition. Finally we conclude in Sect. 5.

2 System description and ZAD strategy

Let us consider the electronic power converter shown schematically in Fig. 1. This kind of device is called a DC/DC buck converter as it reduces a certain input voltage E to another certain voltage v_o which is desired to follow a reference signal ω_{ref} which can be constant or not [12, 13].

As one can see in Fig. 1, the circuit is regulated by a PWM (Pulse Width Modulator) block which switches the system between two topologies shown in Fig. 2. System is in topology A (Fig. 2(a)) during a specific time $T_{\text{on}} = d\,T$, while it is in topology B during $T_{\text{off}} = (1-d)\,T$ seconds. This is repeated every T seconds so that, if the parameter d is constant, then the system has a periodic behavior.

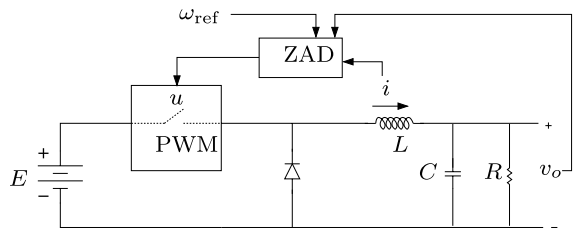

Fig. 1 Schematic representation of the investigated system

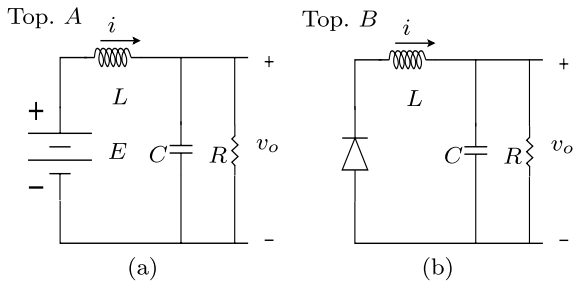

Fig. 2 Switching topologies for the buck converter

Besides the values of the inductor (L), capacitor (C) and resistor (R), the key of the control design in order to make v_o follow the reference signal ω_{ref} is the value of the parameter d. There are many ways to design a control method solving this control problem. The method we consider here is proposed by [9]. It is called ZAD (Zero Average Dynamics) and its goal is to achieve the zero average difference between the output v_o and the desired voltage ω_{ref} and their derivatives in each period T.

2.1 System equations

Let i and v_0 be the current through the inductor and the voltage across the capacitor, also the output voltage, respectively. Taking

$$x_1 = \frac{1}{E} v_o, \qquad x_2 = \sqrt{\frac{L}{C}} \frac{1}{E} i$$

as state variables and rescaling time as

$$t = \frac{\tau}{\sqrt{LC}},$$

the dimensionless system equations can be written in matrix form as

$$\dot{x} = Ax + u, \tag{1}$$

where $x = (x_1, x_2)^T$,

$$A = \begin{pmatrix} -\gamma & 1 \\ -1 & 0 \end{pmatrix}, \qquad \gamma = \frac{1}{R}\sqrt{\frac{L}{C}}$$

and the function

$$u = \begin{cases} B_1 & \text{if } kT \le t \le kT + \frac{1}{2}Td, \\ B_2 & \text{if } kT + \frac{1}{2}Td \le t \le (k+1)T - \frac{1}{2}Td, \\ B_1 & \text{if } (k+1)T - \frac{1}{2}Td \le t < (k+1)T \end{cases} \tag{2}$$

models a central PWM with $B_1 = (0, 1)^T$, $B_2 = (0, 0)^T$ and duty cycle d during the sampling period kT. As one can see from (2), the value d must be in the *feasible interval* [0, 1]. Hereby the value $d = 0$ corresponds to $u = B_2$ (topology B) whereas $d = 1$ corresponds to $u = B_1$ (topology A) for $t \in [kT, (k+1)T]$. We will say that the system gets *saturated* if one of these situations occurs.

2.2 Poincaré map

In order to cover a deeper analysis of the systems behavior, like existence of periodic orbits and bifurcation curves, it is useful to consider the Poincaré map instead of the original flow. As system (1) is non-autonomous but periodic, we can define the Poincaré map as the stroboscopic mapping $P(x_0) := \Phi(T, x_0)$, where $\Phi(t, x_0)$ is the flow of system (1) verifying $\Phi(0, x_0) = x_0$.

As explained in [10], one can additionally take benefit of the linearity of the system (1) to piecewise-integrate it and obtain an explicit expression for the Poincaré map

$$P(x_0, d) = e^{AT} x_0 + \left(e^{AT} - I\right) A^{-1} B_1 + \left(e^{ATd/2} - e^{AT(1-d/2)}\right) A^{-1} B_1. \tag{3}$$

Note that n-periodic orbits of this map discussed in the following are associated with nT-periodic orbits of the original flow. Especially, a fixed point of the Poincaré map corresponds to a T-periodic orbit of the original flow.

2.3 ZAD strategy

As it has been explained in the introduction, in order to make the output of the system v_o to follow a certain desired signal $w_{\text{ref}} > 0$, one can use the ZAD strategy. Setting $v_{\text{ref}} = w_{\text{ref}}/E$ and using the dimensionless variables, as in [6, 7] and [14], one first defines the error surface

$$s(t) := \left(x_1(t) - v_{\text{ref}}\right) + k_s\left(\dot{x}_1 - \dot{v}_{\text{ref}}\right), \tag{4}$$

where parameter k_s is a time constant associated with first order dynamics of the error surface $s(t) = 0$. Taking into account that our choice here is to consider v_{ref} as a constant, (4) can be simplified as

$$s(t) = \left(x_1(t) - v_{\text{ref}}\right) + k_s \dot{x}_1. \tag{5}$$

Once $s(t)$ is defined, the ZAD strategy consists on finding the appropriate value of the duty cycle d for which the function $s(t)$ has zero average at each iteration, that is

$$\int_{kT}^{(k+1)T} s(t)\,dt = 0, \quad \forall k \in \mathbb{Z}. \tag{6}$$

Note, that solving (6) in each iteration corresponds to the closed loop control design which causes the duty cycle d to depend on the state variables at time kT. In the following, this k-dependent duty cycle will be denoted as d_k. As proposed in [10], in order to obtain an analytical expression for d_k one has to rewrite the function $s(t)$ in terms of the flow.

Eliminating $\dot{x}_1$ in (5) using (1), it is easy to see that (6) can be written as the following equation which is transcendental in d_k

$$\begin{aligned} 0 &= \int_{kT}^{(k+1)T} s(t)\,dt \\ &= (1-\gamma k_s, k_s)\int_0^T \Phi(t, x_0, d_k)\,dt - v_{\text{ref}}T, \end{aligned} \tag{7}$$

where the initial condition x_0 represents the value of the system state variables at time kT. The expression of the integral of the flow in (7) is given by

$$\begin{aligned} &\int_0^T \Phi(t, x_0, d_k)\,dt \\ &\quad = TA^{-1}B_1 d_k + A^{-1}\big[\big(e^{AT} - I\big)\big(x_0 + A^{-1}B_1\big) \\ &\qquad + \big(e^{ATd_k/2} - e^{AT(1-d_k/2)}\big)A^{-1}B_1\big]. \end{aligned} \tag{8}$$

Therefore, (7) together with (8) gives an implicit expression which can be solved numerically with respect to d_k at each sampling period although it increases considerably computation costs. As explained for example in [1, 4], in order to avoid solving (7) and (8) and to reduce the complexity of the hardware implementation, one can replace the error surface $s(t)$ defined in (4) by a piecewise-linear function in order to obtain an algebraic expression for the duty cycle

$$\begin{aligned} d_k = {} & \frac{2k_s\gamma - 2 + T(\gamma - k_s(\gamma^2 - 1))}{Tk_s} x_1(kT) \\ & - \frac{2k_s + T(1-k_s\gamma)}{Tk_s} x_2(kT) - \frac{2v_{\text{ref}}}{Tk_s}. \end{aligned} \tag{9}$$

Note that this strategy uses only the values $x_1(kT)$ and $x_2(kT)$ at the beginning of the sampling period instead of using the solution $x_1(t)$ in the whole interval $[kT, (k+1)T]$.

As studied in [1], the average error committed between the real output and the desired one when using this condition is completely acceptable from a practical point of view. However, as we will numerically show in Sect. 4, this leads to some differences with the transcendental one.

From now on, as we will mainly follow [10], we will refer to the transcendental ZAD condition (6) just as ZAD condition.

3 Bifurcation analysis

3.1 Periodic orbits

The strongest foundation of almost all analytical results concerning periodic orbits discussed below is given by the following Lemma:

Lemma 1 (Fossas et al.) *Given a linear system $\dot{x} = Ax + u$ where A is hyperbolic, u is piecewise-linear and L-periodic, such that $\int_0^L u(t)\,dt = 0$, then there exists a unique L-periodic solution $x = x_p(t)$ such that $\int_0^L x_p(t)\,dt = 0$.*

A proof of the Lemma can be found in [10].

Applying a change of variables one can see that the previous Lemma implies the existence of a unique T-periodic solution with $d = v_{\text{ref}} = const$ which fulfills the ZAD condition (see [10] for details). The initial condition x_0^* for this unique T-periodic orbit can be found solving the equation

$$P(x_0, d) = x_0, \tag{10}$$

which explicit expression can be found in [10].

Notice that this result can be extended to nT-periodic solutions as follows. Denoting by

$$x^{\overbrace{*\cdots*}^{n\text{ times}}}_{i,(d_1,\ldots,d_n)} \tag{11}$$

the ith iterated of the Poincaré map of an n-periodic orbit with duty cycles $(d_1, \ldots, d_n)$, the initial condition $x^{*\cdots*}_{0,(d_1,\ldots,d_n)}$ of this orbit is given by the solution of

$$P^n(x_0, d_1, \ldots, d_n) = x_0, \tag{12}$$

where $P^n(x_0, d_1, \ldots, d_n) = P(P(\ldots P(x_0, d_1), \ldots, d_n))$. Applying the Lemma with $L = nT$, it is shown in [10] that the unique nT-periodic orbit with initial conditions $x^{*\cdots*}_{0,(d_1,\ldots,d_n)}$ satisfies the ZAD condition in the whole interval nT if

$$\sum_{i=1}^{n} d_i = n v_{\text{ref}}. \tag{13}$$

In order to guarantee that the ZAD condition is satisfied in each iteration, (7) has to be ensured only for $k = 1, \ldots, n-1$, as it will be automatically fulfilled in the remaining iteration due to condition (13).

As it will be useful below, we give here the corresponding results for the case $n = 2$. In this case the initial condition is given by

$$\begin{aligned} x^{**}_{0,(d_1,d_2)} = &\left(-e^{2AT} + e^{AT(2-d_1/2)} - e^{AT(1+d_1/2)}\right. \\ &\left. + e^{AT(1-d_2/2)} - e^{ATd_2/2} + I\right) \\ &\times \left(e^{2AT} - I\right)A^{-1}B. \end{aligned} \tag{14}$$

As explained above, the ZAD strategy is fulfilled in both iterations of the 2-periodic orbit if both duty cycles d_1 and d_2 satisfy the equations

$$(1 - \gamma k_s, k_s) \int_0^T \Phi\left(t, x^{**}_{0,(d_1,d_2)}, d_1\right) dt - v_{\text{ref}} T = 0, \tag{15}$$

$$(1 - \gamma k_s, k_s) \int_T^{2T} \Phi\left(t, x^{**}_{1,(d_1,d_2)}, d_2\right) dt - v_{\text{ref}} T = 0. \tag{16}$$

However, using $L = 2T$, the Lemma implies that only one of the (15) and (16) needs to be solved. After one of the values d_1, d_2 is calculated, the other one results from the condition

$$d_1 + d_2 = 2v_{\text{ref}}. \tag{17}$$

Note that, as the above Lemma can not be applied, a similar analytical procedure is not possible when using the algebraic ZAD condition. This is why a comparison between both methods will be performed numerically in Sect. 4.

3.2 Period doubling and corner collision bifurcations

As already reported in [10], system (1) undergoes two bifurcations, a usual period doubling and a corner collision bifurcation.

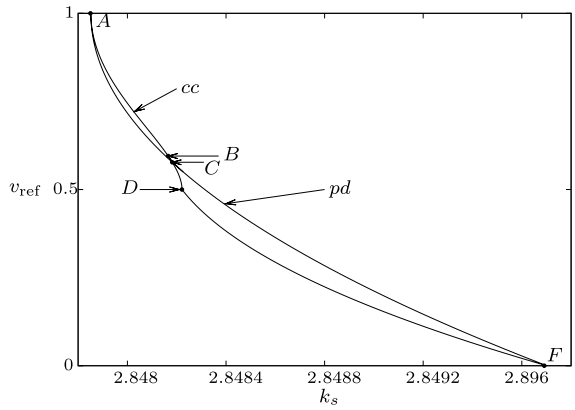

Fig. 3 Period doubling (*pd*) and corner collision (*cc*) bifurcation curves as reported in [10]. Here and in subsequent figures and simulations, the chosen parameters are $\gamma = 0.35$ and $T = 0.1767$

The period doubling bifurcation can be detected using the condition that one of the eigenvalues of the Jacobian of the Poincaré map evaluated at the fixed point equals minus one. So, the expression

$$\det\left(DP\left(x_0^*, d\right) + I\right) = 0, \tag{18}$$

where x_0^* represents the solution of (10) and $d = v_{\text{ref}}$ in order to verify the ZAD condition, leads to the period doubling bifurcation curve. This bifurcation is mentioned in [10] to be a subcritical period doubling. In fact, as we will demonstrate below, it may be a subcritical or supercritical period doubling bifurcation depending on the value of v_{ref}. One of our main goals is to explain how the system undergoes the transition from one case to the other one and which are the differences of the behaviors in both cases. In addition, it will also be shown in Sect. 4 that the period doubling bifurcation is supercritical for all values of v_{ref} when using the algebraic ZAD condition.

With regard to the corner collision bifurcation, as it is explained in [4], it occurs when one of the duty cycles of a 2-periodic orbit reaches the values $d = 1$ or $d = 0$ and the periodic orbit saturates. On the other hand, the Lemma applied to a $2T$-periodic orbit implies $d_1 + d_2 = 2v_{\text{ref}}$ in order to satisfy the ZAD condition in the whole $2T$ period. Therefore, a saturated behavior with the duty cycles $(1, d_2)$ is possible if $v_{\text{ref}} \in [\frac{1}{2}, 1]$ and with the duty cycles $(d_1, 0)$ if $v_{\text{ref}} \in [0, \frac{1}{2}]$. Consequently, the corner collision curve can be calculated for $v_{\text{ref}} \geq \frac{1}{2}$ by (7) using initial condition $x^{**}_{0,(1,d_2)}$, $d_1 = 1$ and $d_2 = 2v_{\text{ref}} - 1$. For $v_{\text{ref}} \leq \frac{1}{2}$

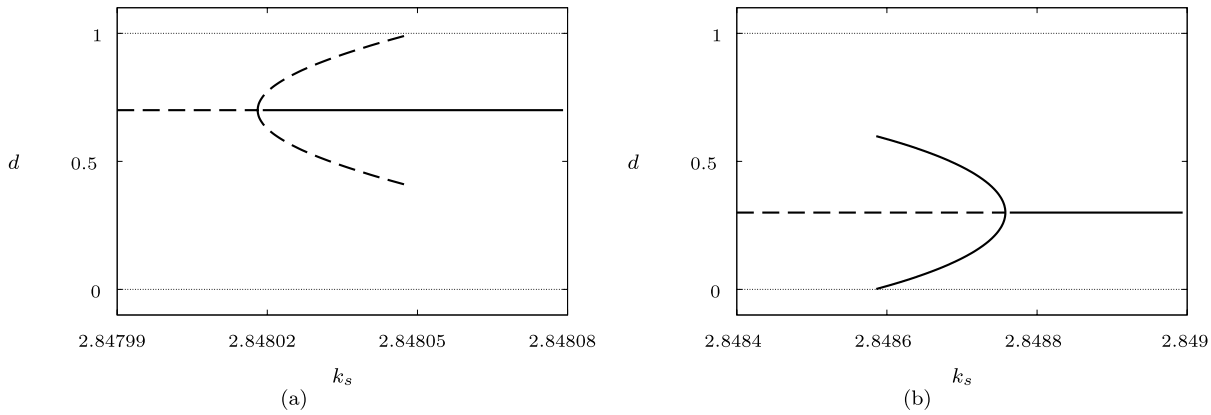

Fig. 4 Subcritical and supercritical period doubling bifurcation at $v_{\text{ref}} = 0.7$ (**a**) and $v_{\text{ref}} = 0.3$ (**b**). *Solid* and *dashed curves* correspond to stable and unstable solutions, respectively

this bifurcation curve results from the same equation with the initial condition $x^{**}_{0,(d_1,0)}$, $d_1 = 2v_{\text{ref}}$ and $d_2 = 0$. The initial conditions $x^{**}_{0,(1,d_2)}$ and $x^{**}_{0,(d_1,0)}$ can be found setting $d_1 = 1$ and $d_2 = 0$, respectively, in (14).

As a consequence, the corner collision bifurcation curve is piecewise-defined. The point D located at $v_{\text{ref}} = \frac{1}{2}$ separates the pieces of this curve defined by different saturation conditions. Note that the corner collision bifurcation curve is non-smooth at this point.

Figure 3 shows the period doubling and the corner collision bifurcation curves described above. As one can see, there exists a crossing point, $C = (k_s^C, v_{\text{ref}}^C)$, between both curves for which both bifurcations occur at the same values of k_s and v_{ref}. As mentioned above, the period doubling bifurcation is either subcritical or supercritical, depending on the value of v_{ref}, as shown[1] in Fig. 4 for values of v_{ref} sufficiently far from v_{ref}^C.

As we will demonstrate below, although C does not separate these two behaviors, it is a codimension-2 bifurcation point and plays an important role for the description of the system's dynamics in the parameter space. On the other hand, points A and F are also codimension-2 points where also both bifurcations occur at the same values of v_{ref} and k_s. However, as it will be clear from further explanations, 2-periodic orbits created by the period doubling at these points are immediately destroyed by the corner collision bifurcation.

[1] Notice that if the ZAD condition is fulfilled, then the behavior of the duty cycle d is more significant for the control strategy than the values of the current and voltage. Due to this we show in Fig. 4 and all bifurcation diagrams below the behavior of d.

Regarding the codimension-2 bifurcation point $B = (k_s^B, v_{\text{ref}}^B)$, it is not given by a crossing point between both curves as will be discussed below.

3.3 Virtual, feasible and saturated periodic orbits

So far, we considered only orbits located at the feasible domain $d \in [0, 1]$. In order to explain the transition between the situations shown in Figs. 4(a) and (b), let us neglect the saturation condition and state the next

Definition A (d_1, d_2) 2-periodic orbit of the Poincaré map (3) is said to be *feasible* if $0 \le d_i \le 1$ for $i = 1, 2$. It is said to be *virtual* or *not feasible* otherwise.

In order to obtain both feasible and virtual orbits let us vary d_1 in $[v_{\text{ref}}, d_{\max}]$, with some $d_{\max} > 1$. Obtaining d_2 from (17) and k_s from (15) or (16), we get for $v_{\text{ref}} > v_{\text{ref}}^B$ the bifurcation diagram shown in Fig. 5(a) where both feasible and virtual orbits are presented. There one can see that the branches of the 2-periodic solution can be better approximated by a fourth-order polynomial instead of a typical parabola. This polynomial can be written as

$$-k_s(d) = a_4(d - v_{\text{ref}})^4 + a_2(d - v_{\text{ref}})^2 + a_0, \qquad (19)$$

and is symmetric with respect to the line $d = v_{\text{ref}}$. Although the coefficients a_0, a_2 and a_4 depend on v_{ref}, in the parameter region we consider the coefficient a_4 is always positive. Point M located at the line $d = v_{\text{ref}}$ corresponds to the period doubling bifurcation. Hence, the type of this bifurcation depends on the sign of a_2.

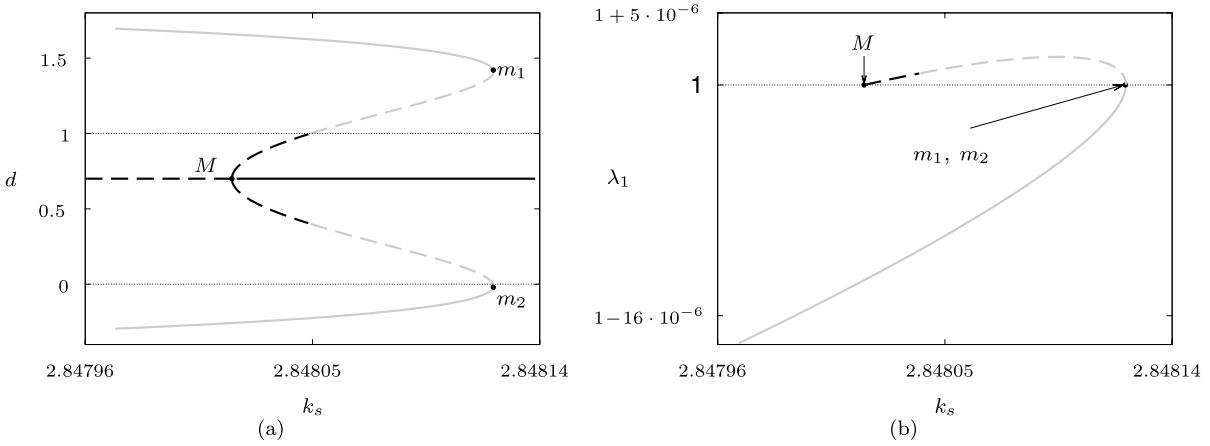

Fig. 5 (**a**) Bifurcation diagram showing both feasible and virtual orbits for $v_{\text{ref}} = 0.7$. (**b**) Critical eigenvalue of $DP^2(x^{**}_{0,(d_1,d_2)})$. *Solid* and *dashed curves* represent, respectively, stability and instability, *black* and *gray curves* show feasible and virtual orbits, respectively

For $a_2 > 0$ the bifurcation is supercritical while for $a_2 < 0$ it is subcritical. In this last case, the function (19) has two additional minima, m_1 and m_2 as shown in Fig. 5(a). Obviously, these points represent a saddle-node bifurcation, but as they are located outside the feasible domain $d \in [0, 1]$ the orbits emerging at these bifurcations are virtual.

The corresponding evolution of the critical eigenvalue of $DP^2(x^{**}_{0,(d_1,d_2)})$ is shown in Fig. 5(b).[2] Notice that this eigenvalue reaches $+1$ not only at the period doubling but also at a saddle-node bifurcation.

In the situation shown in Fig. 5(a), the stable branch remains virtual for all parameter values, whereas the unstable branch reaches the domain [0..1] and becomes feasible via a corner collision bifurcation. Obviously, a variation of v_{ref} not only influences the location of the points m_1, m_2 with respect to the feasible domain [0..1] permitting the stable 2-periodic orbits to become feasible (or to "appear"), but also the shape of the fourth-order polynomial leading the system to different dynamical behaviors. Especially, it is possible that for some other values of v_{ref} the coefficient a_2 changes its sign and the polynomial (19) loses its local minima m_1 and m_2 and therefore the saddle-node bifurcation will be destroyed.

The situation shown in Fig. 5(a) leads us immediately to the following observation. In the right part of this figure the fixed point is stable and, assuming that no other bifurcation occur between the considered ones, the initial values from the complete feasible interval [0, 1] converge to this fixed point. Then the question arises what is the asymptotic dynamics of the system in the left part of the figure, that means in case that the fixed point is unstable. To explain that we have to notice that in this case there exists a stable virtual 2-periodic orbit. Although this orbit is not feasible, it has a basin of attraction and may therefore influence the dynamics. Especially, on the left side of the period doubling bifurcation (point M in Fig. 5) all typical initial values from the interval [0, 1] are attracted by this virtual orbit. However, as the orbits can not leave the feasible interval, they "stick" at its boundary forming a saturated 2-periodic orbit. It is worth noticing that in general the saturated orbits do not represent an invariant set of the underlying flow and emerge only because the orbits have to remain within the feasible domain. As a consequence, these saturated orbits can not be unstable.[3] As one can clearly see in Fig. 5(a), between the period doubling bifurcation and the saddle-node bifurcation the stable fixed point coexists with the stable virtual 2-periodic orbit. To explain which behavior can be observed in this case, note that the basins of attraction of these solutions are separated by the unstable 2-periodic orbit. Therefore, two situations are possible. If the unstable 2-periodic orbit is feasible (on the

[2] One can obtain an analytical expression for $DP^2(x^{**}_{0,(d_1,d_2)})$ from (12) taking into account that d_1 and d_2 depend on x_0 via the ZAD condition at each iteration and applying twice the Implicit Function Theorem.

[3] Note that the behavior in the non-generic cases $v_{\text{ref}} = 0$ and $v_{\text{ref}} = 1$ is different. In this case the fixed point is located at the boundary of the feasible domain and may be stable or unstable.

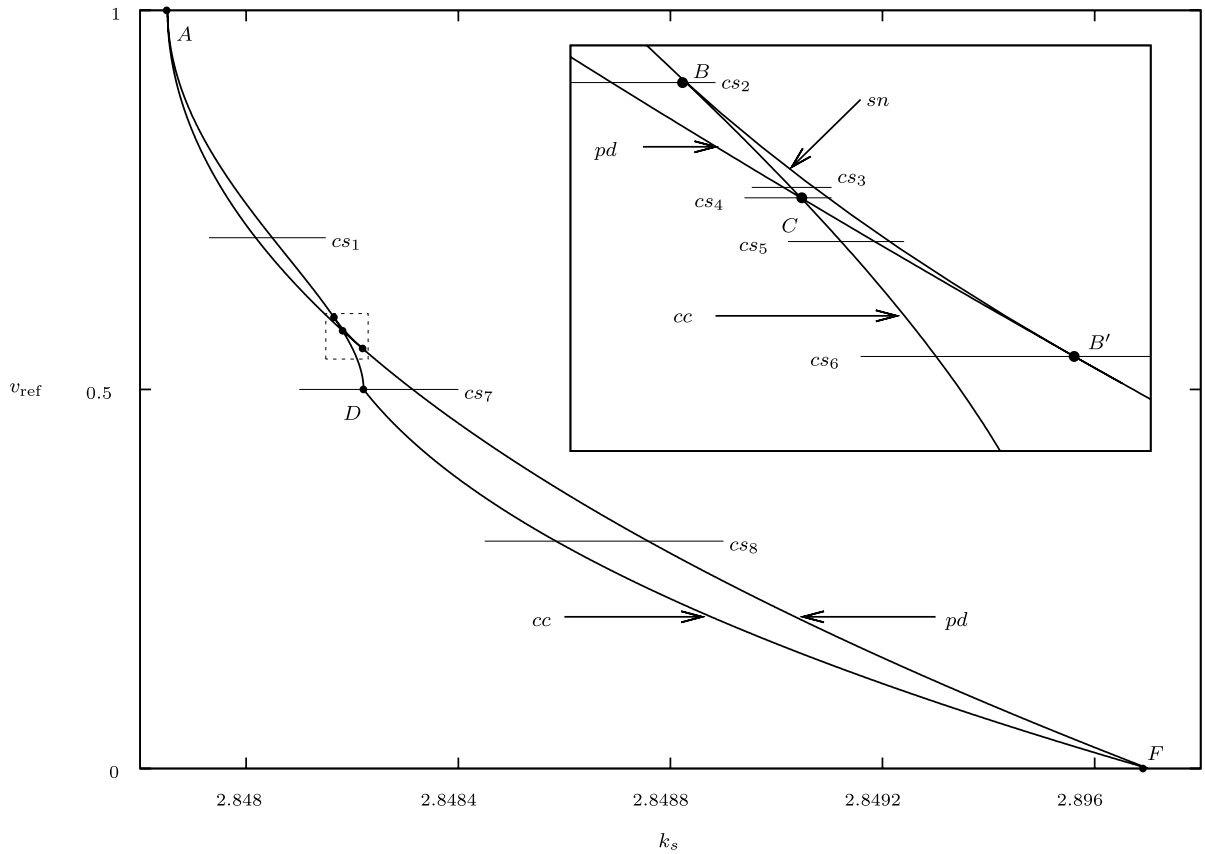

Fig. 6 Period doubling (*pd*), corner collision (*cc*) and feasible saddle-node (*sn*) bifurcation curves. The bifurcation diagrams along the lines marked with cs_i, $i = 1..8$, are shown in Fig. 7. *Inset* shows the *dashed rectangle* enlarged

left side of the corner collision bifurcation), the stable fixed point coexists with a stable saturated 2-periodic orbit. By contrast, if the unstable 2-periodic orbit is virtual (on the right side of the corner collision bifurcation), the basin of attraction of the stable 2-periodic orbit does not reach the feasible domain and therefore the stable fixed point represents the only attractor.

To conclude, we state that orbits in the investigated system can be stable or unstable, feasible or virtual, saturated or not. Transitions between all these behaviors are organized by several points in the two-dimensional parameter space, as described in the next section.

3.4 Bifurcations of virtual and feasible orbits

A variation of v_{ref} leads the positions of the point M (which corresponds to the period doubling bifurcation) as well as of the points m_1 and m_2 (corresponding to the saddle-node bifurcation) to be changed. Recall that point M is located on the symmetry axis of the fourth-order polynomial, which is given by $d = v_{\mathrm{ref}}$. Consequently, as $v_{\mathrm{ref}} \in (0, 1)$, the orbits emerging at the period doubling bifurcation are always feasible. Moreover, for suitable values of v_{ref}, the points m_1 and m_2 may be located in the domain $[0, 1]$. In this case, the orbits undergoing the saddle-node bifurcation are also feasible.

In Fig. 6 additionally to the period doubling and corner collision bifurcation curves also the curve of the saddle-node bifurcation involving feasible orbits is shown. Several characteristic situations of the 2-periodic orbits depending on the shape and location of the fourth-order polynomial are shown in Fig. 7 corresponding to the cross-sections labeled in Fig. 6. Note that Fig. 7 shows also the saturated orbits which occur if the basin of attraction of the stable virtual 2-periodic orbits reaches the feasible domain, as discussed above.

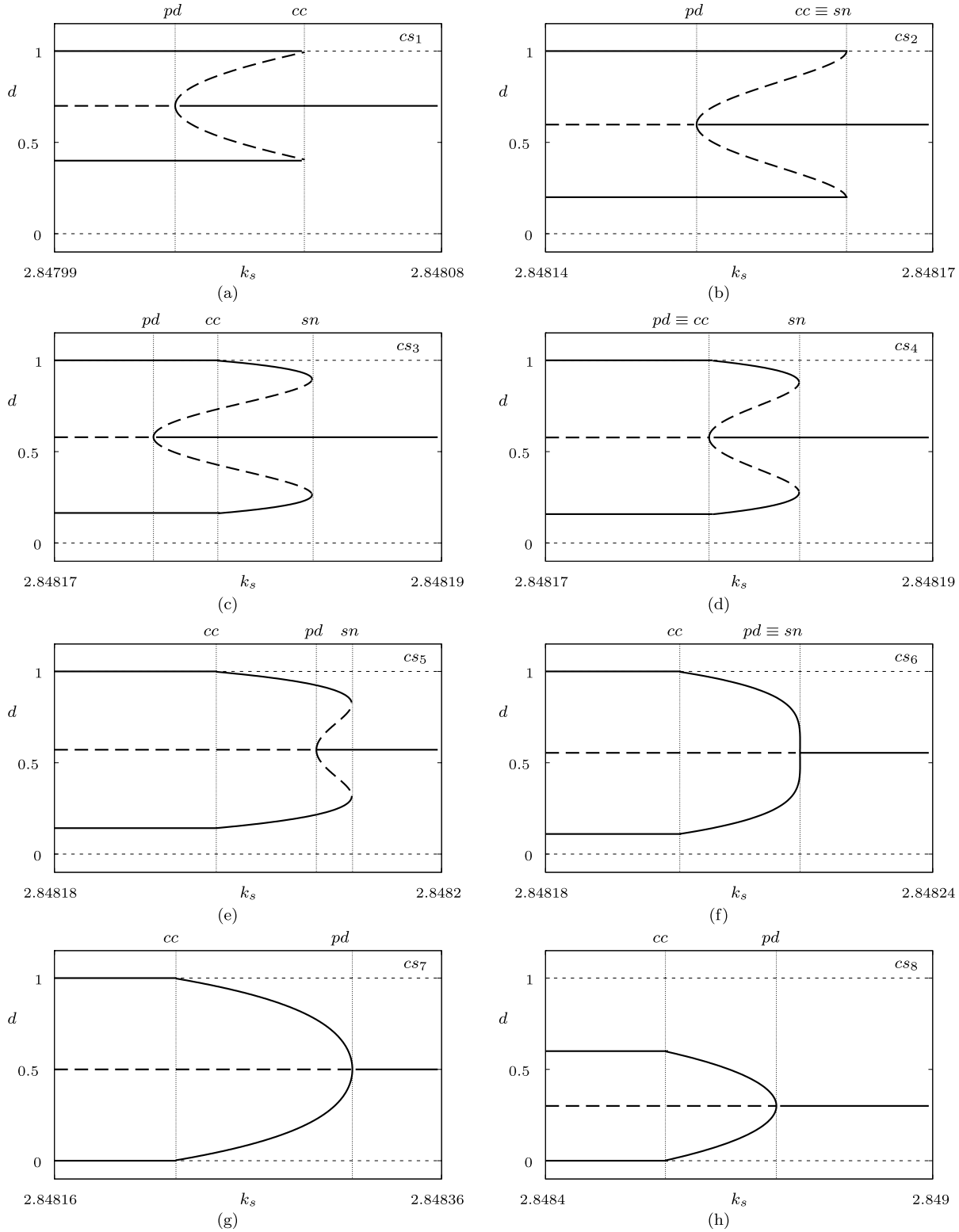

Fig. 7 Bifurcation diagrams corresponding to lines labeled as cs_i, $i = 1..8$, in Fig. 6. Saturated orbits are also shown. Period doubling (*pd*), corner collision (*cc*) and saddle-node (*sn*) bifurcations are marked

First of all, the position of the point M leads us to discuss two different behaviors below and above point D in Fig. 6.

Point D

Due to the symmetry of the fourth-order polynomial with respect to the horizontal line $d = v_{\text{ref}}$, the corner collision bifurcations are different in the cases $v_{\text{ref}} > \frac{1}{2}$ and $v_{\text{ref}} < \frac{1}{2}$. In the first case, 2-periodic orbits become virtual due to the collision of its upper branch with the upper boundary of the feasible region $d = 1$, and one duty cycle of the 2-periodic orbit equals one (the orbit saturates to one). This situation is shown in Figs. 7(a)–(f). By contrast, if $v_{\text{ref}} < \frac{1}{2}$, the lower branch of the 2-periodic orbit collides with the lower boundary of the feasible region and the orbit saturates to zero (Fig. 7(h)).

Obviously, there exists a point, $D = (k_s^D, \frac{1}{2})$, which separates this two different behaviors and where the two branches of the 2-periodic orbit collide with both boundaries of the feasible region at the same value of k_s, so that the orbit after the corner collision bifurcation becomes saturated with duty cycles equal to one and to zero. This case is shown in Fig. 7(g), which corresponds to the cross section cs_7 in Fig. 6.

From Fig. 7 it is also clear, that there exists a value of v_{ref} for which the saddle-node bifurcation points, m_1 and m_2, become feasible. This leads us to discuss the points B and B' marked in Fig. 6.

Points B, B' and the saddle-node bifurcation curve

Recall that in the situation shown in Fig. 5(a), the coefficients a_4 and a_2 in (19) are positive and negative, respectively. As v_{ref} decreases, a_2 increases so that points m_1, M and m_2 become closer. As the period doubling bifurcation point M remains always in the feasible region, there exists a value of v_{ref} for which the points m_1 and m_2 also enter the feasible region so that the orbits emerging at the saddle-node bifurcation become feasible. Therefore, there exists a codimension-2 point labeled as point $B = (k_s^B, v_{\text{ref}}^B)$ where both the saddle-node and the corner collision bifurcation occur for the same value of k_s. This situation is shown in Fig. 7(b), which corresponds to the cross section cs_2 in Fig. 6.

For the values of v_{ref} close but below v_{ref}^B, the saddle-node bifurcation curve becomes feasible and persists until it coincides with the period doubling bifurcation curve at point $B' = (k_s^{B'}, v_{\text{ref}}^{B'})$ labeled in Fig. 6. At that point, the coefficient a_2 reaches zero and points m_1, M and m_2 coincide.

For the values of v_{ref} decreased further, the coefficient a_2 is positive, and since the coefficient a_4 always remains positive, the fourth-order polynomial (19) will lose its two minima. Hence, the saddle-node bifurcation curve disappears for $v_{\text{ref}} \le v_{\text{ref}}^{B'}$. Therefore, point B' is also another codimension-2 bifurcation point where the saddle-node and the period doubling bifurcation occur at the same value of k_s. In other words, the unstable 2-periodic orbit is destroyed if $v_{\text{ref}} \le v_{\text{ref}}^{B'}$ and the period doubling becomes supercritical. This is shown in Fig. 7(f), corresponding to the cross section cs_6 in Fig. 6.

Due to the feasibility of the saddle-node bifurcation points, there exists a region of coexistence of both feasible stable and unstable 2-periodic orbits between points B and B'. This region is bounded by the saddle-node bifurcation curve on the right, and by the period doubling or the corner collision curves on the left, depending on whether v_{ref} is above or below the labeled point C. This last distinction of the left boundaries of the feasible coexistence region leads us to discuss the last point of interest, point C.

Note also that as long as 2-periodic orbits are feasible no attractor is located in the virtual region and, therefore, no saturated orbits are possible as shown in Figs. 7(c)–(h).

Point C

Once the saddle-node bifurcation points m_1, m_2 are located in the feasible region, the point M remains on the left of the corner collision bifurcation point where the orbits become saturated (see Fig. 7(c)). As v_{ref} decreases, point M tends to move to the right while, on the contrary, the collision of the stable branches of the fourth-order polynomial with the boundaries of the feasible region (corner collision) moves to the left (compare Figs. 7(c), (d) and (e)). Before points m_1, M and m_2 coincide as shown in Fig. 7(f), there exists a value of v_{ref} for which the corner collision and the period doubling occur for the same value of k_s. This is the point labeled in Fig. 6 as point $C = (k_s^C, v_{\text{ref}}^C)$. A one-dimensional bifurcation diagram through point C is shown in Fig. 7(d), corresponding to cross section cs_4 in Fig. 6. For v_{ref} decreasing further, the re-

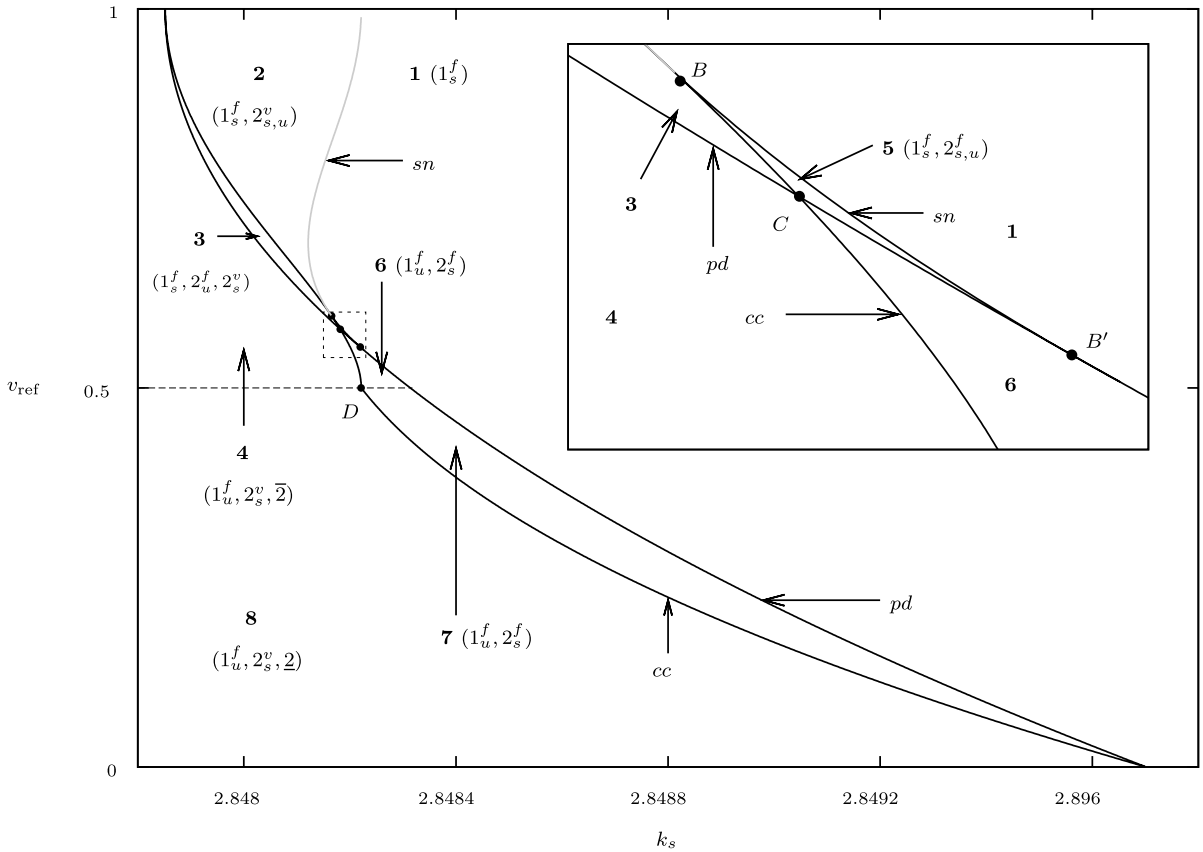

Fig. 8 Regions of existence of several objects bounded by *solid curves*. *Gray curve* represents virtual saddle-node bifurcation. The labels $i^{f/v}_{s/u}$, $i = 1..2$, refer to a feasible/virtual, stable/unstable i-periodic orbit, respectively. $\underline{2}$ and $\overline{2}$ refer to 2-periodic orbit saturated to 1 or to 0, respectively. See text for details

gion of feasible coexistence of both 2-periodic orbits is bounded on the left by the period doubling curve.

Points A and F

There exist also in Fig. 6 two codimension-2 points labeled as A and F with limiting values $v_{\text{ref}} = 1$ and $v_{\text{ref}} = 0$, respectively. There, as the fixed point is located at the boundaries of the feasible domain, the 2-periodic orbits created at the period doubling bifurcation can not be feasible. Hence, for both cases $v_{\text{ref}} = 0$ and $v_{\text{ref}} = 1$, the period doubling bifurcation which causes a 2-periodic orbit to emerge and the corner collision bifurcation which causes this orbit to become virtual occur at the same value of k_s. Note that for these values of v_{ref} all solutions will converge to a saturated fixed point for any value of k_s.

3.5 Regions of existence in parameter space

Based on the results exposed so far, we summarize in Fig. 8 the regions of existence of all 1- and 2-periodic orbits. Note that in this figure the saddle-node bifurcation curve is shown as a gray curve when this bifurcation occurs outside the feasible interval $[0, 1]$ and black otherwise. A dashed horizontal line is also shown to distinguish between the saturation of the 2-periodic orbits to 1 from the saturation to 0. In the following discussions we argue which objects exist in the regions labeled in Fig. 8.

Under some assumptions and using the algebraic ZAD condition, a similar but one-dimensional study has been performed numerically in [5] for two and higher-period orbits.

Regions 1 and 2

In these regions only the stable fixed point is feasible. The only difference between the Regions 1 and 2 is given by the fact that in the first case there are no 2-periodic orbits, whereas in the second case there exists a stable and an unstable 2-periodic orbit created at the saddle-node bifurcation. However, these orbits are virtual and do not influence the dynamics in any way (see Figs. 5(a) and 7(a)). Especially, since the unstable virtual 2-periodic orbit and hence the basin of attraction of the stable one are located outside the feasible domain, no saturated orbits are possible in Region 2. Hence, in both Regions 1 and 2 all initial values are attracted by the stable fixed point.

Region 3

This region is confined by the period doubling and the corner collision bifurcation curves above point C. Therefore, in this region a stable fixed point coexists with an unstable feasible 2-periodic orbit and with a stable virtual 2-periodic orbit. As the unstable 2-periodic orbit is feasible, the basin of attraction of the virtual stable 2-periodic orbit intersects the feasible region, and therefore the stable fixed point coexists in this region with a 2-periodic orbit saturated to one (see also Fig. 7(a)).

Regions 4 and 8

These regions are bounded on the right hand side by the period doubling above C and by the corner collision bifurcation curve below this point. As only the unstable fixed point is feasible and no unstable 2-periodic orbits exist there, all orbits are attracted to the boundaries of the feasible region by the stable virtual 2-periodic orbits. Therefore, all typical initial values in both regions converge towards saturated 2-periodic orbits. Depending on whether $v_{\text{ref}} > \frac{1}{2}$ or not, the orbits saturate to 1 (Region 4) or to 0 (Region 8). As stated above, for $v_{\text{ref}} = \frac{1}{2}$ the orbits saturate to both values, to 0 and to 1 (see Fig. 7(g)).

Region 5

This region is bounded on the right side by the saddle-node bifurcation curve, and, on the left one, by the corner collision bifurcation curve above point C and by the period doubling bifurcation curve below. There coexist three different objects and all of them are feasible: stable and unstable 2-periodic orbits and the stable fixed point (see Figs. 7(c)–(e)). Therefore, solutions using values of k_s and v_{ref} located in that region could converge to the stable fixed point or to a stable 2-periodic orbit with non-saturated duty cycles. As stated above, no saturated orbits exist in this region because the stable 2-periodic orbit is feasible.

Regions 6 and 7

Below point C and between the period doubling and the corner collision bifurcation curves, the fixed point is unstable, the stable 2-periodic solutions are feasible and the unstable 2-periodic ones do not exist (see Figs. 7(f)–(h)). Therefore, all typical orbits with parameters located in this region will converge to a non-saturated 2-periodic orbit as it is the unique attractor that exists there.

The only reason to distinguish between the Regions 6 and 7 regards the properties of the stable 2-periodic orbit. For values of v_{ref} larger (smaller) than $\frac{1}{2}$, that is in the Region 6 (7), the stable 2-periodic orbit is located close to the upper (lower) boundary of the feasible domain. This means that the upper (lower) branch of the 2-periodic orbit collides with the boundary of the feasible domain at the corner collision bifurcation, which leads to an orbit saturated to one (zero).

4 Numerical simulations

Let us compare the analytical results reported above with the numerical results when simulating the system for two different situations, for $v_{\text{ref}} = 0.7$ where the system undergoes a subcritical period doubling bifurcation (Fig. 7(a)) and for $v_{\text{ref}} = 0.3$ where the period doubling bifurcation is supercritical (Fig. 7(h)). It will also be shown for the first case, how the dynamics is qualitatively different when considering the algebraic ZAD condition described in Sect. 2.3.

The results presented in this section have been obtained by iterating the Poincaré map (3) using the same initial condition for several values of k_s and a fixed value of v_{ref}. At each iteration, (7) has been solved using a Newton–Raphson method in order to find the value of d which satisfies the ZAD condition at the current iteration.

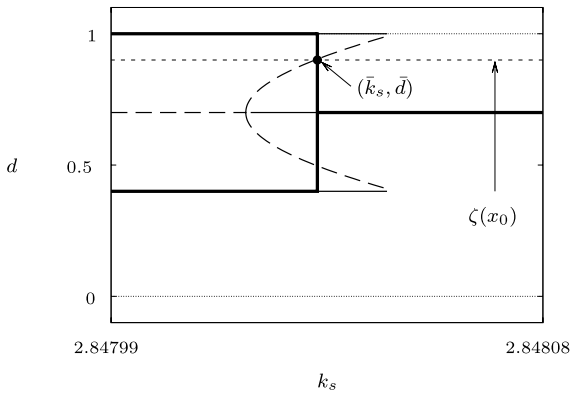

Fig. 9 Expected results for $v_{\text{ref}} = 0.7$

From what has been exposed in previous sections, it is clear that, when trying to simulate the system for v_{ref} such that the saddle node is not feasible (see Fig. 7(a)), a 2-periodic orbit with one saturated duty cycle should be obtained for k_s located on the left hand side of the period doubling bifurcation. It is also clear that the fixed point should be obtained for k_s located on the right hand side of the corner collision bifurcation. However, for k_s between these two bifurcations both stable objects coexist (Region 3 of Fig. 8), so the asymptotic dynamics in this region depends on the fact to which basin of attraction the initial duty cycle belongs to. As d is not a state variable but is related with them through the ZAD condition, let us consider the family of curves $\zeta(x_0)$ formed by points (k_s, d) such that, for a certain initial condition x_0, the ZAD condition is fulfilled in the first interval, that means in $[0, T]$,

$$\zeta(x_0) = \Big\{ \big(k_s, d(x_0, k_s)\big) \mid (1 - \gamma k_s, k_s) \times \int_0^T \Phi(t, x_0, d)\, dt - v_{\text{ref}} T = 0 \Big\}.$$

This curve is shown in Fig. 9 for a certain value of x_0.

Let us denote with $(\bar{k}_s(x_0), \bar{d}(x_0))$ the point given by the intersection of this curve with the unstable 2-periodic branch for a certain x_0. As for $k_s > \bar{k}_s$ the orbit is attracted to the fixed point and for $k_s < \bar{k}_s$ to the 2-periodic orbit with one saturated duty cycle, a jump between the fixed point and the saturated 2-periodic orbit is expected to occur for $k_s = \bar{k}_s$ when numerically investigating the system, as shown in Fig. 9. Note that the curve $\zeta(x_0)$ shown in Fig. 9 looks like a constant function. In fact it is not, but some

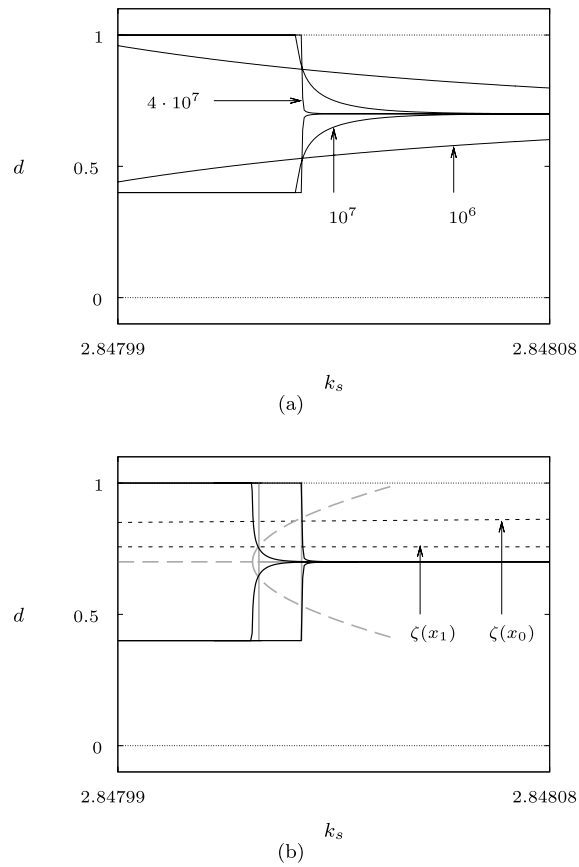

Fig. 10 Simulations for $v_{\text{ref}} = 0.7$. (**a**) Simulations using 10^6, 10^7 and 4×10^7 iteration steps. (**b**) Simulations for two different initial conditions. In *gray* the expected jump and the analytical unstable orbit, in black the obtained numerical results after 4×10^7 iteration steps

calculations show that $|\partial d(x_0, k_s)/\partial k_s| \ll 1$ and hence the function is almost constant.

Figure 10(a) shows the results of numerical simulations calculated for $v_{\text{ref}} = 0.7$, using 10^6, 10^7 and 4×10^7 iteration steps. As one can clearly see, for the calculation of the bifurcation diagrams a large number of iterations is required. However, for increasing number of iterations the bifurcation diagram calculated numerically gets closer to the one predicted analytically. Consequently, we observe the *critical slowing down* effect; that is, the closer k_s gets to $\bar{k}_s$, the slower the dynamics is. This is because an orbit using an initial value in a small vicinity of the unstable 2-periodic orbit which separates the basins of two coexisting attractors, needs more iteration steps to leave this vicinity as the vicinity gets smaller. This is the reason why practically instead of the predicted jump a smooth transition

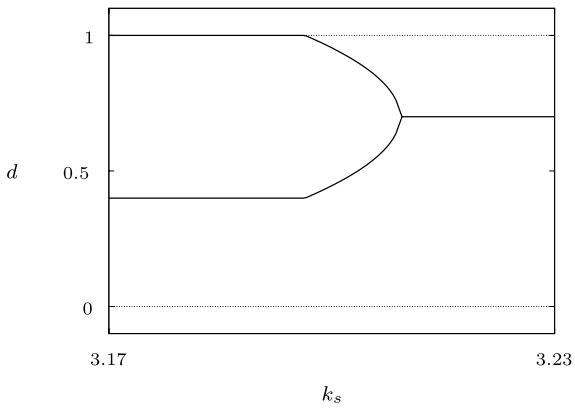

Fig. 11 Bifurcation diagram using the piecewise-linear approximation of $s(t)$

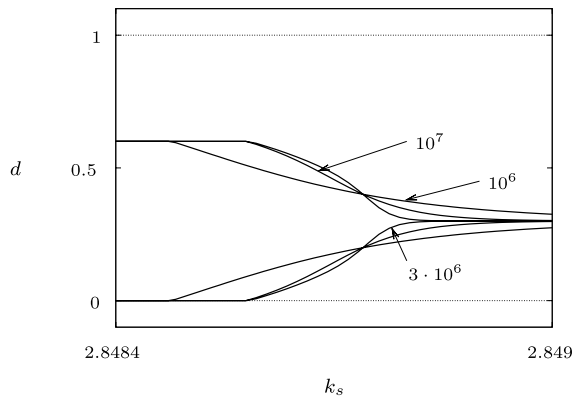

Fig. 12 Simulations for $v_{\text{ref}} = 0.3$ using 10^6, 3×10^6 and 10^7 iterations

from the fixed point to the saturated 2-periodic orbit will be observed, as can be clearly seen in Fig. 10(a). Especially the results obtained using only 10^6 iteration steps are far from the expected ones.

As already indicated in Fig. 9, the value of k_s where the jump between the fixed point and the saturated 2-periodic orbit occurs, that is $\bar{k}_s$, depends on the used initial condition. Figure 10(b) shows the results obtained numerically using two different initial conditions and confirms this result.

Let us finally emphasize that all analytical results discussed above concern the system verifying the transcendental ZAD condition exactly. As mentioned in previous sections, when the error surface $s(t)$ is replaced by a piecewise-linear function in order to obtain a closed expression for the duty cycle (algebraic ZAD condition), one obtains qualitatively different results as the described above. Especially, using the same parameter values and initial conditions as in Fig. 10, we obtain for the map using (9) to compute the duty cycle d, the results shown in Fig. 11 (see also [4, 5]). As shown in this figure, the saddle-node bifurcation and the subcritical structure of the period doubling bifurcation no longer exist. Instead, a supercritical period doubling bifurcation is detected. Remarkably, this holds for all values of v_{ref} and hence, when using the algebraic ZAD condition, the period doubling bifurcation curve will be detected on the right hand side of the corner collision bifurcation curve in parameter space for all values of v_{ref}.

From previous sections it is clear that when simulating the system for $v_{\text{ref}} = 0.3$, that means below point D in Fig. 6, a supercritical period doubling bifurcation will be detected. Fig. 12 confirms this result and demonstrates again the critical slowing down effect.

5 Conclusions

We reported a procedure which provides an analytical description of the bifurcation structures occurring in linear systems with a piecewise-linear nonautonomous periodic control. The procedure was based on the lemma about periodic orbits in these systems recently given in [10]. We applied this procedure to the fixed points and 2-periodic orbits in a buck converter controlled by the ZAD strategy.

It was demonstrated that depending on the value of the parameter v_{ref}, the period doubling bifurcation in this system may be both subcritical and supercritical. Considering feasible and virtual orbits we showed that the investigated system undergoes also a saddle-node bifurcation. For many parameter values the 2-periodic orbits emerging at this bifurcation are virtual and hence will be not observed. However, we detected the codimension-2 bifurcation point where the saddle-node bifurcation becomes feasible. This allowed us to detect a region in the parameter space where a stable fixed point coexists with non-saturated 2-periodic orbits. We also showed that the transition between the subcritical and the supercritical period doubling bifurcations occurs at the codimension-2 point (not reported until now) where additionally a saddle-node bifurcation is destroyed.

We presented a unified description of all codimension-2 bifurcation points involving fixed points and

2-periodic orbits. This allowed us to determine the regions of existence of all one- and two-periodic objects, both stable and unstable, saturated and non-saturated.

The results obtained analytically were confirmed using numerical simulations. It turned out that the behavior of the investigated system is strongly influenced by the critical slowing down effect. Additionally, we compared our results with the results reported in [4], where a piecewise-linear surface is used to perform the ZAD condition and compute the duty cycle. We showed numerically that, in that case, the period doubling bifurcation is supercritical for all parameter values. Consequently, both transcendental and algebraic ZAD conditions lead to significant different bifurcation structures, mainly given by different relative position of the bifurcation curves.

References

1. Angulo, F.: Análisis de la dinámica de convertidores electrónicos de potencia usando PWM basado en promediado cero de la dinámica del error (ZAD) (Spanish). Ph.D. thesis, Universitat Politècnica de Catalunya (2004)
2. Angulo, F., Fossas, E., Olivar, G.: Transition from periodicity to chaos in a pwm-controlled buck converter with zad strategy. Int. J. Bifurc. Chaos **15**(10), 3245–3264 (2005)
3. Angulo, F., Ocampo, C., Olivar, G., Ramos, R.: Nonlinear and nonsmooth dynamics in a DC-DC Buck converter: Two experimental set-ups. Nonlinear Dyn. **46**, 239–257 (2006)
4. Angulo, F., Olivar, F.G., Di Bernardo, M.: Two-parameter discontinuity-induced bifurcation curves in a ZAD-strategy-controlled DC-DC buck converter. IEEE Trans. Circ. Syst. I **55**, 2392–2401 (2008)
5. Angulo, F., Olivar, G., Taborda, A.: Continuation of periodic orbits in a ZAD-strategy controlled buck converter. Chaos Solitons Fractals **38**, 348–363 (2008)
6. Bilalović, F., Mušić, O., Šabanović, A.: Buck converter regulator operating in the sliding mode. In: Proceedings VII International PCI, pp. 331–340 (1983)
7. Carpita, M., Marchesoni, M., Oberti, M., Puguisi, L.: Power conditioning system using slide mode control. In: Proceedings of the IEEE Power Electronics Specialist Conference, pp. 623–633 (1988)
8. Di Bernardo, M., Budd, C.J., Champneys, A.R., Kowalczyk, P.: Piecewise-Smooth Dynamical Systems: Theory and Applications. Applied Mathematical Sciences, vol. 163. Springer, Berlin (2007)
9. Fossas, E., Griñó, R., Biel, D.: Quasi-sliding control based on pulse width modulation, zero average dynamics and the l_2 norm. In: Yu, X., Xu J.-X. (eds.) Advances in Variable Structure Systems. Analysis, Integration and Applications, pp. 335–344. Proceedings of the VI IEEE International Workshop on Variable Structure Systems, Gold Coast, Australia, 7–9 December 2000. World Scientific, New York (2000)
10. Fossas, E., Hogan, S.J., Seara, T.M.: Two-parameter bifurcation curves in power electronic converters. Int. J. Bifurc. Chaos **19**, 341–357 (2009)
11. Krein, P.T., Bentsman, J., Bass, R.M., Lesieutre, B.L.: On the use of averaging for the anallysis of power electronic systems. IEEE Trans. Power Electron. **5** (1990)
12. Mohan, N., Undeland, T.M., Robbins, W.P.: Power Electronics: Converters, Applications, and Design. Wiley, New York (2002)
13. Severns, R., Bloom, G.: Modern DC to DC Switch-Mode Power Converter Circuits. Springer, Berlin (1985)
14. Venkataramanan, R., Sabanovic, A., Cuk, S.: Sliding mode control of DC-to-DC converters. In: Proceedings IECON, pp. 251–258. California, 18–22 November 1985. Pub. the Institute (1985)